



Cite this: *Soft Matter*, 2017, 13, 8756

## Arrested and temporarily arrested states in a protein–polymer mixture studied by USAXS and VSANS†

Stefano Da Vela,<sup>a</sup> Christian Exner,<sup>a</sup> Richard Santiago Schäufele,<sup>a</sup> Johannes Möller,<sup>b</sup> Zhendong Fu,<sup>c</sup> Fajun Zhang<sup>\*a</sup> and Frank Schreiber<sup>id a</sup>

We investigate the transition of the phase separation kinetics from a complete to an arrested liquid–liquid phase separation (LLPS) in mixtures of bovine  $\gamma$ -globulin with polyethylene glycol (PEG). The solutions feature LLPS with upper critical solution temperature phase behavior. At higher PEG concentrations or low temperatures, non-equilibrium, gel-like states are found. The kinetics is followed during off-critical quenches by ultra-small angle X-ray scattering (USAXS) and very-small angle neutron scattering (VSANS). For shallow quenches a kinetics consistent with classical spinodal decomposition is found, with the characteristic length ( $\xi$ ) growing with time as  $\xi \sim t^{1/3}$ . For deep quenches,  $\xi$  grows only very slowly with a growth exponent smaller than 0.05 during the observation time, indicating an arrested phase separation. For intermediate quench depths, a novel growth kinetics featuring a three-stage coarsening is observed, with an initial classical coarsening, a subsequent slowdown of the growth, and a later resumption of coarsening approaching again  $\xi \sim t^{1/3}$ . Samples featuring the three-stage coarsening undergo a temporarily arrested state. We hypothesize that, while intermittent coarsening and collapse might contribute to the temporary nature of the arrested state, migration-coalescence of the minority liquid phase through the majority glassy phase may be the main mechanism underlying this kinetics, which is also consistent with earlier simulation results.

Received 19th July 2017,  
Accepted 5th November 2017

DOI: 10.1039/c7sm01434a

[rsc.li/soft-matter-journal](http://rsc.li/soft-matter-journal)

## 1 Introduction

The study of phase transitions in protein solutions is a flourishing research field. On the one hand, it is a topic of fundamental interest as proteins represent the small size limit for colloids and feature peculiar effects due to shape and interaction anisotropy.<sup>1–4</sup> On the other hand, this research field is closely related to a wide range of applications, including formulation and stability of biopharmaceuticals,<sup>5</sup> protein crystallization,<sup>6</sup> biomaterials,<sup>7</sup> and industrial food processing.<sup>8,9</sup> Recently, much attention has been devoted to the study of liquid–liquid phase separation (LLPS) in protein solutions.<sup>4,10–14</sup> In particular, it was found that in

colloid and protein systems interacting with a short-ranged attractive potential, the interplay of spinodal decomposition with glass formation during the LLPS can prevent a complete phase separation, resulting in an arrested state.<sup>15–24</sup>

Usually the kinetics of spinodal decomposition is described by the Cahn–Hilliard theory.<sup>25</sup> In essence, the theory predicts the amplification of concentration fluctuations during phase separation, with a characteristic wavelength being selected by the balance of interface tension and diffusion along the gradient of chemical potential. Experimentally, this is reflected by the growth of a peak in the structure factor  $S(q)$ , which can be measured by small-angle scattering. As coarsening sets in, the peak continues to grow in intensity and its position,  $q_{\max}$ , shifts to lower values of the scattering vector  $q$ .<sup>25–27</sup> The growth kinetics of the characteristic length  $\xi = 2\pi/q_{\max}$  is customarily divided in successive stages, with different growth exponents for its time dependence.<sup>27,28</sup> The coarsening process at later stages is a multifaceted phenomenon,<sup>29,30</sup> with numerous mechanisms possibly concurring to the observed growth law.<sup>31,32</sup> Hydrodynamic and gravitational effects become important in the late stage of coarsening,<sup>26,33</sup> and can also affect the arrested LLPS.<sup>34–37</sup> Systems in the arrested state have been shown to still undergo some form of residual coarsening.<sup>38–41</sup>

<sup>a</sup> Institut für Angewandte Physik, Universität Tübingen, Auf der Morgenstelle 10, 72076 Tübingen, Germany. E-mail: fajun.zhang@uni-tuebingen.de; Fax: +49 7071-29 5110; Tel: +49 7071-29 75242

<sup>b</sup> European Synchrotron Radiation Facility, 71 avenue des Martyrs, 38043 Grenoble Cedex 9, France

<sup>c</sup> Forschungszentrum Jülich GmbH, JCNS@MLZ, Lichtenbergstrasse 1, 85747 Garching, Germany

† Electronic supplementary information (ESI) available. See DOI: 10.1039/c7sm01434a

‡ Present address: European XFEL GmbH, Holzkoppel 4, 22869 Schenefeld, Germany.

§ Present address: Neutron Scattering Laboratory, Department of Nuclear Physics, China Institute of Atomic Energy, 102413 Beijing, China.

**Table 1** Composition and volume fraction ( $\phi$ ) of the dense phase samples used for USAXS and VSANS experiments, obtained by equilibration at 21 °C of the corresponding parent solutions

Sample	$[\gamma\text{-Globulin}]$ in dense phase ( $\text{mg mL}^{-1}$ )/ $\phi\%$	[PEG] in dense phase (%w/v)	$[\gamma\text{-Globulin}]/[\text{PEG}]$ parent solution ( $\text{mg mL}^{-1}$ )/(w/v)
Sample I	$220 \pm 29/16 \pm 2$	$3.8 \pm 1.2$	110/9
Sample II	$232 \pm 29/17 \pm 2$	$4.3 \pm 0.9$	110/10
Sample III	$246 \pm 22/18 \pm 1$	$4.4 \pm 0.4$	150/9
Sample IV	$295 \pm 31/22 \pm 2$	$2.7 \pm 1.1$	150/10

So far, only a few protein systems have been studied with respect to the kinetics of LLPS and its interplay with glass formation.<sup>8,15,42–44</sup> Lysozyme has been used as a model system for this purpose. Studies indicate that the dynamic arrest of lysozyme solution undergoing LLPS can lead to three scenarios, depending on the quench depth. For shallow quenches (in the so-called “region I”,<sup>42</sup> not to be confused with the denomination of the samples in Table 1) LLPS proceeds to completion, for intermediate quenches (“region II”) the dynamic arrest prevents the full LLPS, and for very deep quenches (“region III”) a homogeneous attractive glass is formed.<sup>8,15,42</sup> These findings have recently been discussed using a non-equilibrium theory of arrested spinodal decomposition,<sup>45</sup> accounting for the behavior observed in colloid and protein solutions.<sup>8,15,42,46</sup> The Mode Coupling Theory (MCT) is often used to predict the location of a glass line. However an experimental study has shown the lack of absolute arrest of the dynamics even beyond the MCT line,<sup>47</sup> and the relation between the glass line and the binodal is still a matter of debate.<sup>15,17–24</sup> Despite these recent advances, scarce experimental data is available for the kinetics of LLPS at quench depths corresponding to the crossover between region I and II.

In our previous work, we have successfully applied ultra small-angle X-ray scattering (USAXS) and very small-angle neutron scattering (VSANS) to study the kinetics of LLPS in a protein–salt system exhibiting a lower critical solution temperature (LCST) phase behavior.<sup>44</sup> We followed the phase transition from sub-second to  $10^4$  s upon an off-critical temperature jump. For shallow quenches, the growth of the characteristic length  $\xi$  follows a power law close to  $\xi \sim t^{1/3}$  up to the first 300 s, which is consistent with coarsening mechanisms based on diffusion or coalescence.<sup>32</sup> For deep quenches, the growth of the characteristic length initially follows the  $t^{1/3}$  power law (for about the first 30 s), but then slows down and is practically stationary, indicating an arrested state.

In this work, we study the kinetics of LLPS and its arrested state in mixtures of bovine  $\gamma$ -globulin and PEG, which exhibits an upper critical solution temperature (UCST) phase behavior. In this system, a short-range attractive “depletion” interaction is provided by the non-adsorbing polymer PEG. Compared with many other proteins such as lysozyme and serum albumin,  $\gamma$ -globulins have a more branched and flexible structure. Indeed, for antibodies, the binodal of LLPS has a critical volume fraction much lower than the one of globular proteins, due to their non-spherical and anisotropic nature.<sup>4,48</sup> These features make antibodies particularly attractive to explore the kinetics of phase separation. Furthermore, studies on the LLPS of monoclonal antibodies in concentrated solutions are crucial for the pharmaceutical industry.<sup>5,49–51</sup> Bovine  $\gamma$ -globulin used in this work

is a polyvalent antibody mixture and the effective interactions are dominated by short-ranged attractions as demonstrated in previous work.<sup>52</sup> By adding a non-absorbing polymer such as PEG, a tunable depletion interaction enhances the protein–protein attraction and leads to LLPS under a broad range of experimental conditions. For exceedingly strong attractive interactions, arrested states can be observed.<sup>4,53</sup> We focus in particular on the coarsening kinetics approaching the arrested state. The results are discussed in comparison with our previous work on BSA as well as other globular protein systems.

## 2 Experimental

### 2.1 Materials and sample preparation

Bovine  $\gamma$ -globulin (purity  $\geq 99\%$ , Sigma-Aldrich, SRE0011), PEG 1000 (Sigma-Aldrich, 81188), NaCl (Merck 106404), HEPES (Roth, HN78) and  $\text{NaN}_3$  (Sigma-Aldrich, S8032) were used as received. All solutions were prepared in a buffer of composition 20 mM HEPES pH = 7.0, 2 mM  $\text{NaN}_3$ , using degassed Milli-Q water (Merck Millipore 18.2 M $\Omega$  cm). The solutions for the evaluation of phase behavior and the samples for USAXS and VSANS experiments were mixed from buffer and stocks solutions (in buffer) of  $\gamma$ -globulin, PEG 1000 36% (w/v) and NaCl 4 M, to a final NaCl concentration of 150 mM. The concentration of the  $\gamma$ -globulin stock solutions was assessed by UV absorption at 280 nm, employing an extinction coefficient<sup>54</sup>  $E_{280} = 1.4 \text{ mg}^{-1} \text{ mL cm}^{-1}$  with a Cary 50 UV-Vis spectrophotometer.

High volume fraction samples were prepared starting from compositions in the LLPS region of the phase diagram. These “parent solutions” were equilibrated for about 12 h at 21 °C and then briefly centrifuged, resulting in clear dense and dilute phases, separated by a sharp meniscus. The dense phases obtained were isolated and used for USAXS and VSANS measurements. The protein and PEG concentrations for these samples were determined from the protein and PEG concentration in the corresponding dilute phases measured by UV absorption and refractive index measurements, respectively. For the refractive index measurement an Abbe refractometer (Krüss AR4), calibrated with Milli-Q  $\text{H}_2\text{O}$ , was employed. Standard curves for  $\gamma$ -globulin and PEG 1000 in 20 mM HEPES pH = 7.0, 2 mM  $\text{NaN}_3$ , 150 mM NaCl were used to correct for the protein contribution and to determine the PEG concentration. The volume of the dilute phase was evaluated by pipetting, and the concentrations in the corresponding dense phase were calculated from mass conservation.

## 2.2 Determination of phase behavior

The state of solutions containing  $\gamma$ -globulin and PEG 1000 was determined by visual inspection of samples mixed at different composition and equilibrated for about 24 h at 21 °C. The binodal for an initial composition 110 mg mL<sup>-1</sup>  $\gamma$ -globulin, 10% (w/v) PEG 1000 was determined equilibrating the samples in a water bath (at least 6 h) at the desired temperature. Samples were prepared in triplicates in PCR tubes. The protein concentration in the dilute phases was assessed by measuring the UV absorption at 280 nm using a NanoDrop 1000 spectrophotometer (Thermo Scientific) after completing the sedimentation by a brief centrifugation step. The volume of the dilute phase was determined by pipetting and the protein concentration in the dense phase was calculated from mass conservation. Extending the equilibration time alters the phase diagram only slightly. We must mention that the phase boundaries seem to shift to lower PEG concentrations and to higher temperatures depending on the age of the starting lyophile. This kind of shift in protein solutions was reported in other protein systems and linked to oxidation.<sup>55</sup>

Mass concentrations were converted to volume fractions using the specific volume of  $\gamma$ -globulin (0.739 mL g<sup>-1</sup>).<sup>56</sup>

## 2.3 Time-resolved USAXS

Time-resolved USAXS experiments were performed at the ESRF beamline ID02 in Grenoble, France.<sup>57</sup> Using a sample-detector distance of 30.7 m and an X-ray energy of 12.46 keV ( $\lambda = 0.099$  nm) it was possible to cover a  $q$  range of  $9.0 \times 10^{-4}$  nm<sup>-1</sup> to  $7.5 \times 10^{-2}$  nm<sup>-1</sup> ( $q$  is the scattering vector defined as  $q = (4\pi/\lambda)\sin\theta$ ,  $2\theta$  is the scattering angle). A fast-readout low-noise (FReLoN<sup>58</sup>) fibre-optic coupled CCD detector in a  $1 \times 1$  binning mode was used for data collection. Samples were filled in 1.0 mm quartz capillaries and inserted horizontally in a Linkam temperature-controlled sample environment with a set heating and cooling rate of 80 K min<sup>-1</sup>.

Initially the samples were equilibrated in the single-phase state at 38 °C, then quenched to the desired temperature. The scattering profiles were followed in time acquiring successive exposures of 30 ms. Measurements for each quench were repeated three times to follow the phase separation with sufficient time resolution at initial, intermediate and long times. For the initial time range (up to 36 s from the first acquisition) scattering profiles were acquired every 0.56 s, every 5 s for the intermediate time range (up to ~5 min), and every 30 s for the long time range (up to ~15 min). Between measurements, the sample was brought back to the single-phase state at 38 °C and the capillary was shifted to illuminate a different position to reduce the radiation damage. The  $t = 0$  profile was collected after a short time delay (15 to 30 s) that compensates for the time needed to reach the set temperature given the heating rate and the quench depth selected. The times for the subsequent profiles were obtained from the time stamps associated with the detector images. Scattering profiles collected at 38 °C before and after every measurement were used for monitoring the reversibility and stability of the samples, and for background subtraction.

To identify the position of the peak in the structure factor, a computer script smoothing the scattering profiles and searching for the maximum intensity was employed.<sup>44</sup>

## 2.4 Time-resolved VSANS

The focusing mirror instrument KWS-3 operated by JCNS at the Heinz Maier-Leibnitz Zentrum (MLZ), Garching, Germany<sup>59</sup> was employed for time-resolved VSANS experiments. Using a neutron wavelength of 1.28 nm with  $\Delta\lambda/\lambda = 20\%$  and a sample-to-detector distance of 9.3 m, a  $q$ -range from about  $3.7 \times 10^{-4}$  to  $1.1 \times 10^{-2}$  nm<sup>-1</sup> was covered. The scattered intensity was collected using a <sup>6</sup>Li-scintillation detector with pixel size of  $0.116 \times 0.116$  mm<sup>2</sup>, size  $3 \times 3$  cm<sup>2</sup> and a deadtime of 2.9  $\mu$ s without beamstop. The beam size at the entrance aperture was  $0.7 \times 0.7$  mm<sup>2</sup>, the beam size at the sample cell was  $8 \times 8$  mm<sup>2</sup>. Samples in 1 mm quartz cells were first equilibrated in the single-phase state in a water bath and then placed in the temperature-controlled sample environment at the desired final temperature. The kinetics at long times was followed by collecting 12 successive exposures of 10 min. Scattering profiles obtained from the samples as single phases at 35 °C were used as backgrounds. The peak position was found on the radially integrated data by smoothing and searching for the maximum of the scattering peak. VSANS data were reduced on absolute intensity with the program QtiKWS provided by JCNS.<sup>60</sup>

# 3 Results

## 3.1 Phase behavior: the binodal of LLPS

The phase behavior of the  $\gamma$ -globulin/PEG 1000 mixture was investigated. The radius of gyration of the depletant (PEG 1000) was reported to be 1.34 nm in a moderate ionic strength aqueous buffer,<sup>61</sup> and the radius of gyration of an IgG-type monoclonal antibody, 5.2 nm,<sup>62</sup> can be considered the lower limit for the radius of gyration of  $\gamma$ -globulin. This results in a depletant-to-protein size ratio of 0.26. Depletion interactions are then short ranged, and the LLPS is in principle metastable with respect to the fluid-crystal coexistence.<sup>63,64</sup> Furthermore, crystallization is not an issue given the polyvalent nature of  $\gamma$ -globulin and its broad distribution of isoelectric points. The effective protein-protein interactions are dominated by a short-ranged attraction as demonstrated in our previous study.<sup>52</sup>

In Fig. 1a we show the state diagram at constant temperature as a function of protein and PEG concentration. A boundary separating clear and turbid solutions can be crossed by increasing PEG concentration at a given protein concentration. Turbid samples prepared in the vicinity of this boundary fall in a region corresponding to LLPS, and eventually undergo macroscopic separation into two transparent liquid phases. Non-equilibrium states are observed at higher PEG concentrations, as the strength of the depletion interaction is further increased.

Based on the state diagram, we chose a composition of 110 mg mL<sup>-1</sup>  $\gamma$ -globulin and 10% w/v PEG 1000 to study the temperature dependence of the phase behavior. Fig. 1b shows a binodal in the protein concentration-temperature plane.

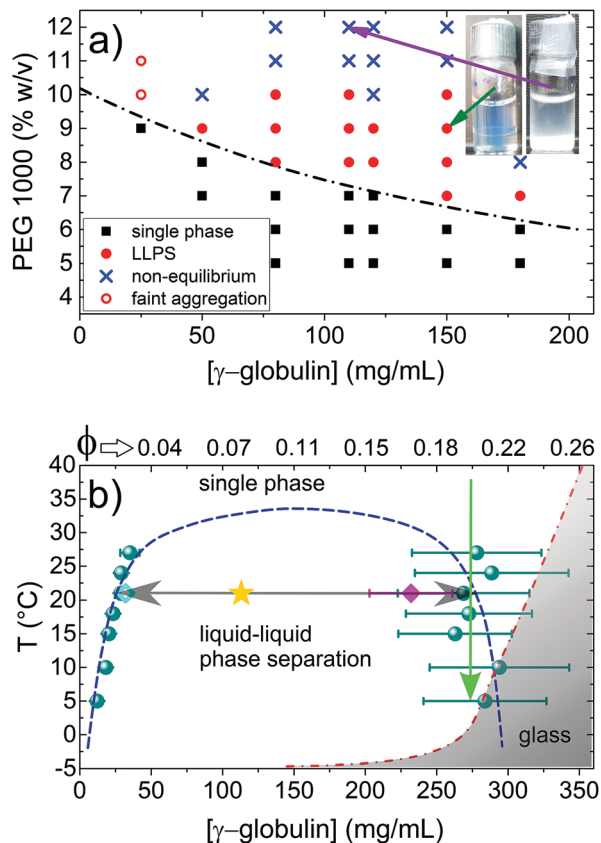


**Fig. 1** (a) State diagram for  $\gamma$ -globulin in the presence of PEG 1000 at 21 °C. The dashed-dotted line is a boundary between single-phase and two-phase solutions. The inset shows two typical phase-separated samples representing the full LLPS and the non-equilibrium gel-like state. The sample conditions are indicated by the arrows. (b) Binodal of the LLPS for a parent solution with 110 mg mL<sup>-1</sup>  $\gamma$ -globulin and 10% (w/v) PEG 1000 (sample II in Table 1). The dashed and the dash-dotted lines are a guide to the eye for the LLPS binodal and for the glass line, respectively. A parent solution (star symbol) undergoes a first phase separation at 21 °C (gray horizontal arrow), resulting in a dilute and a dense phase (diamond symbols). The green vertical arrow indicates a typical off-critical quench.

Long-lived non-equilibrium states manifest at low temperatures as clearly gel-like dense phases, indicating the vicinity of the glass line, which potentially affects the shape of the binodal. The values of the volume fraction of protein ( $\phi$ ) are also labeled on the top axis of Fig. 1b. The high concentration branch of LLPS binodal has a maximum volume fraction about 0.22 (290 mg mL<sup>-1</sup>) which is much lower than that (about 0.35) for globular proteins as lysozyme<sup>42</sup> and  $\gamma_B$ -crystallin.<sup>43</sup> This difference may be due to the “Y” shape of these protein molecules. Studies on monoclonal antibodies have shown a critical volume fraction of about 0.086, much lower than that for hard sphere systems or globular proteins.<sup>4,65</sup>

The compositions of the samples used for USAXS and VSANS (samples I–IV) are reported in Table 1, together with the composition of the corresponding parent solutions. In Fig. 1b we show the composition of sample II, of its parent solution (star symbol) and of the corresponding dilute phase. The difference in protein concentration between sample II and the binodal might be due

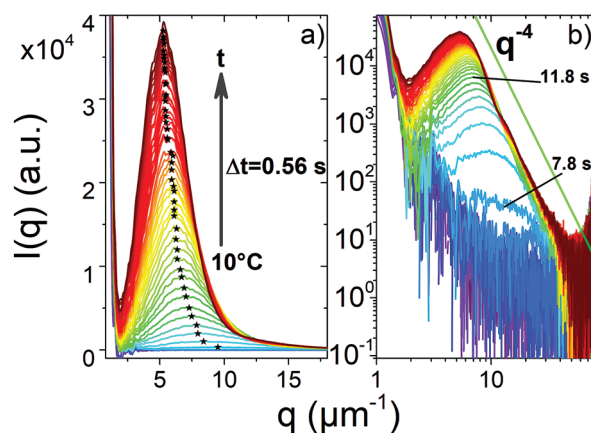
to the aging of the protein lyophile. A typical off-critical quench of the isolated dense phase, as employed in the scattering experiments, is indicated by the green arrow. During such a quench, the high protein volume fraction sample undergoes a further LLPS, which at sufficiently low temperatures can kinetically arrest due to the interference of the glass transition of the newly formed majority dense phase.

### 3.2 Kinetics of phase separation

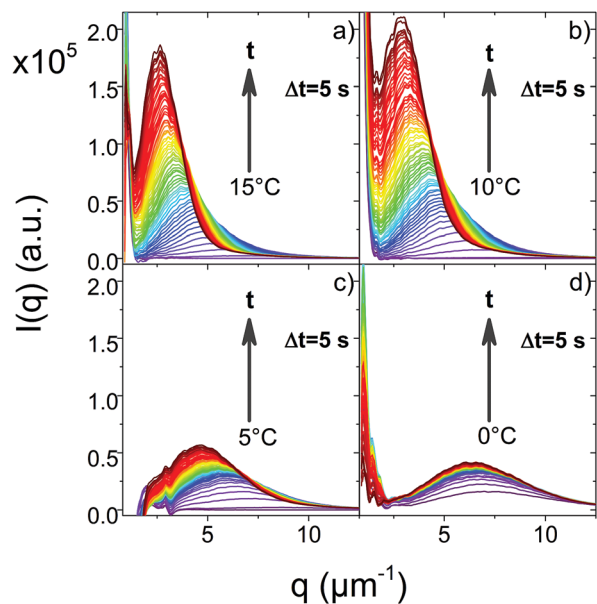
Samples I–IV (Table 1), selected to study the phase transition kinetics, lie on the dense branch of the binodal at the preparation temperature (21 °C). Cooling these samples results in an off-critical quench, and the samples demix into a new dense phase (majority phase) and a new dilute phase (minority phase). The majority phase in these conditions can be brought closer to the glass line the lower the temperature of the quench, producing a kinetically arrested state.

Fig. 2 shows the typical USAXS profiles during the initial stage of LLPS for a temperature quench from 38 to 10 °C of sample II. The structure factor features a peak with position  $q_{\text{max}}$ , which increases in intensity and shifts to lower values of  $q$  as coarsening sets in. The initial development of the peak is better appreciated in the logarithmic plot (Fig. 2b). The first clearly visible peak occurs after 7.3 s and increases in intensity. After 11.8 s the intensity decays at high  $q$  as  $q^{-4}$ , indicating that a well-defined interface is established. In all measurements, the early “linear” stage predicted by the Cahn–Hilliard model,<sup>25,27</sup> where the peak position is constant and the peak maximum grows in intensity, is not observed within the time resolution employed.

Fig. 3 shows USAXS data at intermediate times for the same sample (sample II), with increasing quench depths (decreasing temperatures). Lowering the quench temperature from 15 °C to 10 °C results into a slower shift of the peak maximum to low  $q$ , while the intensities of peaks corresponding to the same times



**Fig. 2** Typical USAXS profiles following the phase separation at early times ( $t \leq 36$  s) in (a) linear scale and (b) logarithmic scale, for sample II undergoing a quench to 10 °C. The peak in the scattering intensity increases in intensity and moves to lower values of  $q$  as the sample phase separates. The stars mark the assigned peak maxima (see text). The green line in the logarithmic plot is a  $q^{-4}$  slope. Profiles collected every 0.56 s.



**Fig. 3** USAXS profiles collected every 5 s, following the phase separation at intermediate times (up to  $t \approx 5$  min) for the same sample as in Fig. 2. Increasing the quench depth (lower temperatures) slows down the peak evolution. For the deepest quench, the phase separation arrests and after a few seconds the peak is stationary. Quenches from 38 °C to (a) 15 °C, (b) 10 °C, (c) 5 °C and (d) 0 °C.

after the quench are higher. This is consistent with a quench to a deeper region of the binodal, where the concentration difference between the two phases is higher, resulting in higher contrast. Further lowering the temperature of the quench below 10 °C, the growth of the peak severely slows down and its position becomes almost stationary at later times for the lowest temperature.

The long-term coarsening behavior was studied by VSANS. The minimum accessible  $q$  is lower ( $3.7 \times 10^{-4} \text{ nm}^{-1}$ ), allowing to detect the peak maximum even after hours from the start of the quench. A larger volume can be sampled, and radiation damage is essentially absent. The exact same samples as for USAXS, in a light water-based buffer, can be measured using VSANS. Typical VSANS profiles for samples III (Fig. 4a–c) and IV (Fig. 4d) are shown at different quench temperatures, with time resolution of 10 min. Again, for a given composition, it is observed that lowering the quench temperature leads to the slowdown, and eventually to the arrest, of the growth. The sample at higher overall protein concentration features the almost arrested kinetics already at higher temperatures.

The combination of USAXS and VSANS allows to follow the evolution of the characteristic length  $\xi = 2\pi/q_{\text{max}}$  for more than three orders of magnitude in time. Fig. 5 shows the evolution of  $\xi$  for sample III at two temperatures. Fig. 5a is relative to a quench depth featuring a temporary slowdown before a resumption of the phase separation. In this case, USAXS and VSANS data correspond well. The power law of  $\xi \sim t^{1/3}$  for diffusive growth represents reasonably the data after an initial slowdown. At even later times a hint of a linear growth,  $\xi \sim t$ , is visible, indicative of a hydrodynamic-dominated growth.<sup>32</sup> An essentially stationary

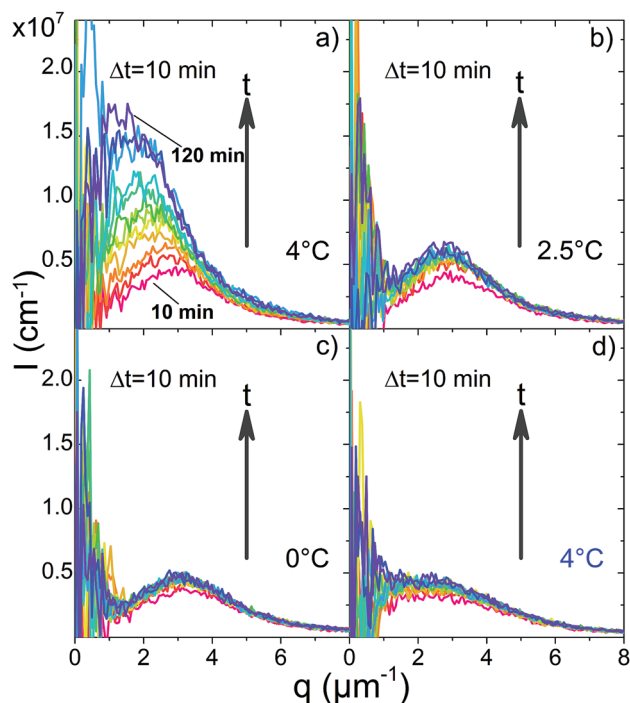


**Fig. 4** Long time structural evolution (up to 120 min) of samples (a–c) III and (d) IV, followed by VSANS while undergoing LLPS. The quench temperature for each time series is shown next to the corresponding scattering peak. The sample at higher protein volume fraction shows the arrested kinetics already at higher temperatures. For all the profiles, data are integrated every 10 min.

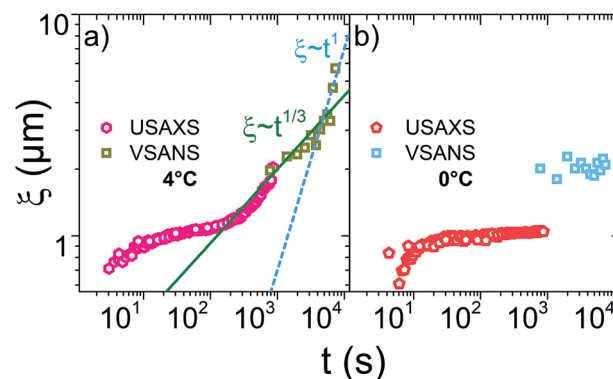


**Fig. 5** Characteristic length as a function of time, jointly showing USAXS and VSANS data, for sample III at two temperatures. (a) Quench to 4 °C. The continuous line and the dashed line show a  $\xi \sim t^{1/3}$  and a  $\xi \sim t$  trend as a guide to the eye. They correspond to a diffusive coarsening and a possible coarsening with hydrodynamic effect, respectively. (b) Quench to 0 °C. The characteristic length does not grow significantly, and the mismatch for the stationary  $\xi$  value could be due to a temperature gradient in the larger VSANS cell.

value of  $\xi$  is confirmed by both techniques for the lowest temperature probed, a consequence of the dynamical arrest. The value of the characteristic length, however, is found to differ between USAXS and VSANS. We ascribe this discrepancy to heat transmission in the larger VSANS cells, resulting in an effectively higher temperature for this sample.

### 3.3 Temporarily arrested state

The temporal evolution of  $\xi$  as a function of time for all four samples (I–IV) and for increasing quench depths is shown in Fig. 6. Sample I (Fig. 6a), having the lowest overall protein concentration, shows only a minor slowdown of the growth in the temperature range probed, and a fully arrested state is not reached. For samples with either higher PEG concentration (II and III) or higher protein concentration (IV), a significant slowdown and the arrested kinetics can be observed (Fig. 6c and d).

Interestingly, the coarsening behavior visible for intermediate temperature quenches is not expected. The growth kinetics first obeys the  $1/3$  power law, followed by a clearly visible slowdown. The duration of this slowdown depends on the sample and on the quench temperature. Then, surprisingly, the coarsening resumes with a growth exponent again close to  $1/3$ . This non-monotonic kinetics for the coarsening is observed already at higher temperatures for samples with higher protein volume fractions. For sample I, this non-monotonic kinetics is only observed at the lowest temperatures. For a given sample, the resumption of the coarsening occurs at later times for deeper quenches, and eventually is no longer observed within the experimental time window (about 15 min). Furthermore, the growth exponent during the slowdown decreases with increasing quench depths as well. Therefore, this coarsening behavior can be described as a “three-stage” process: an initial coarsening, a slowdown plateau

and a resumption of the coarsening. We thus denote the conditions featuring this type of kinetics as being in a temporarily arrested state. This behavior can be appreciated for instance in Fig. 6 for sample III at  $4^\circ\text{C}$  or sample IV at  $6^\circ\text{C}$ , with the latter showing clearly a temporarily arrested state between 30 s and 100 s from the start of the quench. Another interesting observation in Fig. 6 is that the values of  $\xi$  at the early stage (for  $t < 10$  s) seem to increase for increasing quench depth. This observation is at variance with previous results on lysozyme where  $\xi$  decreases for increasing quench depths.<sup>42</sup> We speculate that, for very deep quenches, diffusion-limited fractal aggregation might start to play a role, affecting the mechanism for dynamical arrest.<sup>16</sup> Further studies are desirable to experimentally determine the transition from the deeply quenched LLPS to the aggregation regime.

To quantify the growth kinetics, growth exponents were extracted in the 30–90 s time range, in which the slowdown stage is seen for all samples. The exponents are summarized in Fig. 7, as a function of the quench depth  $\Delta T$ , defined as the difference between the temperature at which the samples cross the binodal ( $21^\circ\text{C}$ ) and the quench temperature. For sample I, the exponent is initially constant ( $\approx 0.3$ ), then it decreases almost linearly with increasing  $\Delta T$ . For the other three samples, the growth exponent also starts with a value around 0.3 and decreases immediately as the quench depth is increased. However, for these samples (II–IV), for  $\Delta T > 17^\circ\text{C}$ , the decrease of the exponent becomes slower, approaching final values  $\leq 0.05$ . These results show that the transition from the full phase separation to the arrested phase separation is smooth. An analogous gradual decrease of the growth exponent was reported for colloid–polymer mixtures approaching gelation.<sup>37,40</sup> It is worth noting that the slowdown at intermediate times does not correspond to the early stage kinetics of spinodal decomposition where a growth exponent as low as of  $1/6$  can be expected.<sup>19,66</sup> In our case, a typical coarsening with a growth exponent of  $1/3$  occurs before

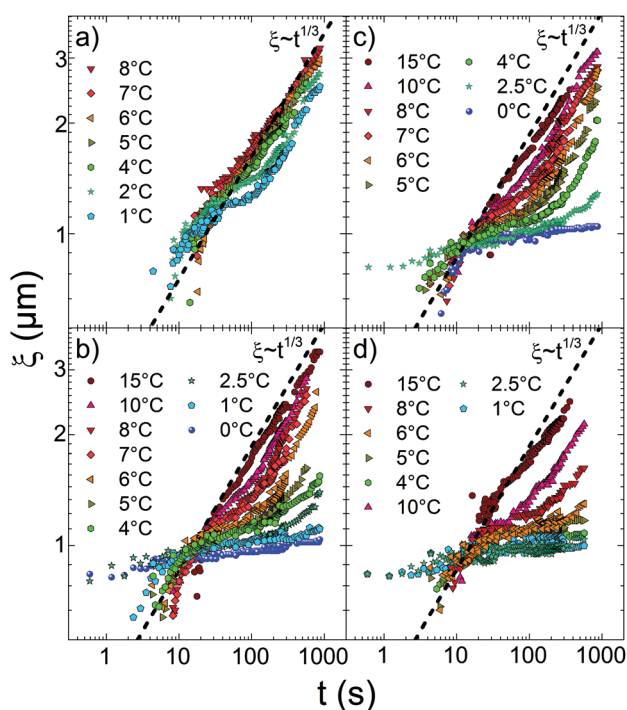


Fig. 6 Development of the characteristic length as a function of time for samples I (a), II (b), III (c), and IV (d), as extracted from time-resolved USAXS experiments. The dashed lines represent a  $\xi \sim t^{1/3}$  growth law. Higher protein volume fraction samples feature a stronger deviation from the classical coarsening behavior, up to temporary and long-lasting arrest, for a given temperature range.

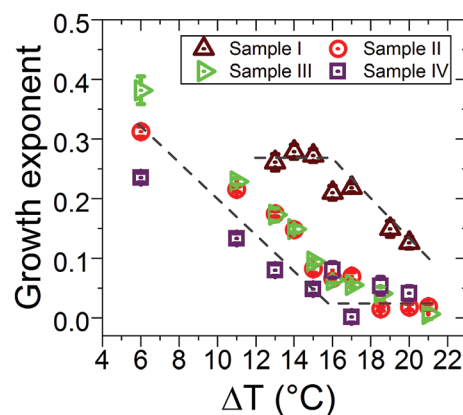


Fig. 7 Growth exponents as a function of the quench depth  $\Delta T$ , defined as the temperature difference between the binodal and the quench temperature  $T$ :  $\Delta T = 21^\circ\text{C} - T$ . For all the samples and temperatures, the  $\xi(t)$  curves were fitted in the range 30 s to 90 s, which excludes the initial stage and the resumption of the coarsening for the deeply quenched samples. Higher dense phase volume fractions generally result in slower growth at a given temperature. The dashed lines are a guide to the eye.

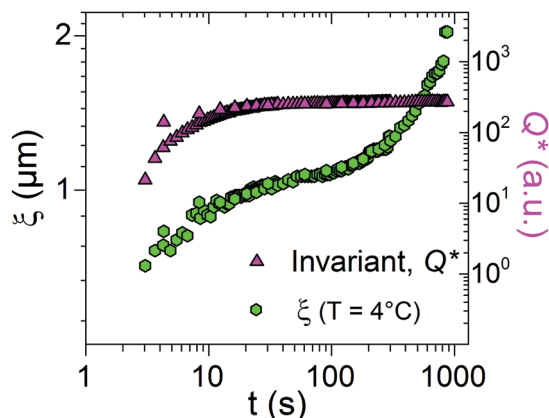


Fig. 8  $\xi(t)$  for sample III quenched to 4 °C, overlaid with the time evolution of a Porod-like scattering invariant,  $Q^*$ , calculated with an integration range 1.8 to 30  $\mu\text{m}^{-1}$ .  $Q^*$  remains constant as the coarsening resumes. A constant  $Q^*$  also argues against major gravity-driven collapse, as it also implies constant relative volume of the two phases.

and after this slow down. During this temporary slow down, the system may behave like a “transient gel”.<sup>67</sup>

For better understanding the resumption of the coarsening, we calculated a Porod-like scattering invariant, as shown in Fig. 8 together with  $\xi(t)$ , for sample III quenched to 4 °C. The invariant is calculated as  $Q^* = \int_a^b q^2 I dq$ , with  $a$  and  $b$  the lowest and highest  $q$  values chosen to define the integration range (here 1.8 to 30  $\mu\text{m}^{-1}$ ). This approximates the Porod invariant  $Q$ , which, for a two phase system, can be shown to be<sup>68</sup>  $Q = 2\pi^2\phi(1 - \phi)\Delta\rho^2$  where  $\Delta\rho$  is the scattering contrast, related to the concentration difference in the two phases, and  $\phi(1 - \phi)$  is the product of the volume fractions occupied by the two phases. The invariant suggests that the final composition compatible with the quench temperature is reached at the initial stage and maintained throughout the three-stage coarsening. This implies that the increase of  $\xi$  at the late stage is purely a coarsening phenomenon, changing only the spatial distribution of the two phases. Their relative amounts and concentrations stay constant, regardless of whether the final composition corresponds to equilibrium or to an arrested non-equilibrium state.

## 4 Discussion

Our experiments show a clear slowdown of the growth kinetics for deep off-critical quenches in the LLPS binodal. Sufficiently deep quenches determine a substantially arrested phase separation kinetics. The growth exponent at the intermediate stage decreases with the quench depth as shown in Fig. 7. In the deeply quenched regime, where the exponents are below 0.05, the system is in a gel-like arrested state. In analogy with colloidal systems,<sup>40</sup> we expect in this case the volume fraction and interactions in the dense phase to be such that the overall dynamics is dominated by the global dynamics of the individual proteins in the dense phase. A novel coarsening behavior becomes evident at quench depths intermediate between full phase separation and dynamical arrest. In a previous study<sup>44</sup>

we investigated the kinetics of LLPS and dynamical arrest in a different protein system in which short-range attractive interactions were induced by addition of  $\text{YCl}_3$ , resulting in a LCST-LLPS. In that study we occasionally observed for intermediate quench depths an analogous growth kinetics featuring slowdown and a resumption of the coarsening. One example is shown in Fig. S1, ESI,† of the present work. This peculiar coarsening, present both in a LCST and in a UCST system, is then probably not affected by the details of the interaction. Instead, it may be a rather general phenomenon.

Therefore, the physical mechanisms underlying the novel three-stage coarsening and the temporary arrest deserve a further discussion. We will in the following describe two possible mechanisms for the observed growth kinetics, which may not be mutually exclusive.

The first possible mechanism to be considered is the temporarily arrested state exhibiting still a slow intermittent dynamics, with residual coarsening resulting from the relaxation of mechanical stresses in the aging (glassy) majority phase.<sup>41,69</sup> Here we assume that the dense phase has retained a network-like structure from the early stage of the spinodal decomposition, characterized by weak points in its connectivity. This slow growth would then be rapidly accelerated again when  $\xi$  reaches the capillary length<sup>33</sup> resulting in gravitational collapse and further coarsening of what is left of the original network. Transient gelation and gravitational collapse have been observed in both long<sup>34,37</sup> and short-range attraction<sup>36</sup> colloid-polymer mixtures. In the case of the  $\gamma$ -globulin/PEG 1000 system, on the other hand, there are three results arguing against a major gravitational collapse. First, the coarsening resumes rather gradually. Second, the spinodal “ring” (corresponding to the correlation peak) in the 2D scattering pattern does not disappear and remains isotropic (Fig. S2, ESI†), in contrast with previous findings on collapse.<sup>33,34</sup> Third, the scattering invariant (shown in Fig. 8) does not decrease during the resumption of the coarsening, as instead would be expected for a removal of dense phase from the scattering volume due to sedimentation. Nevertheless, we cannot completely exclude the relaxation of stresses under gravity as having a role in the observed three stage coarsening.

The second possible mechanism is specific to off-critical quenches. In this case the morphology at later stage is assumed to consist of droplets of minority phase dispersed in a glassy matrix. A droplet morphology can also emerge from initially network-like structures.<sup>32</sup> Two-dimensional simulations<sup>39</sup> including a concentration-dependent mobility in the Cahn-Hilliard equation resulted in a glassy majority phase surrounding more dilute droplets. This system still undergoes coarsening, by apparent migration and coalescence of the enclosed droplets. This movement is based on dissolution of the glassy matrix on one side of the dilute droplet and deposition on the opposite side. This implies a certain degree of heterogeneity of the glassy matrix. Strikingly, this coarsening mechanism results in a three-stage behavior rather similar to the one presented in the present work. In the simulation, the three-stage coarsening is more or less pronounced depending on the choice of the functional

form of the mobility function, in particular of how it approaches the glass transition. This interpretation stresses the role of interfaces for the dynamic of fluid inclusions in non-ergodic matrices. Indeed, even for liquid lead inclusions moving in crystalline aluminum an analogous mechanism of dissolution and coalescence has been reported.<sup>70,71</sup> It is worth noting that although these results are relative to 2D systems, a similar mechanism mediated by higher mobility at the interface may apply also in 3D systems and provide a mechanism for coarsening in the arrested state.

A picture which could potentially combine the coarsening *via* interface-enhanced mobility with the aging and collapse scenario is provided in a confocal microscopy study of colloid-polymer systems with medium and long range attractive interactions.<sup>40</sup> In this study, the authors also found a gradual decrease in growth exponents when increasing polymer concentration, approaching dynamical arrest. While a resumption of the coarsening such as the one found in the present work was not observed, a locally enhanced mobility for particles at the network interface was seen in arrested samples, by tracking the local dynamics of the colloids. It was suggested that the higher mobility could be promoted by the relaxation of mechanical stresses. In addition to the kinetic information reported in our work, further studies of the dynamics of the proteins approaching the arrested state would certainly benefit the understanding of these phenomena.

## 5 Conclusions

We have presented a systematic study on the kinetics of LLPS in a protein-PEG system exhibiting UCST phase behavior. USAXS and VSANS allow to access a broad range of time and length scales and to follow the phase transition kinetics. Solutions of bovine  $\gamma$ -globulin in the presence of PEG 1000 can be quenched to a two-phase state by lowering the temperature. For sufficient protein concentration and sufficiently deep quenches arrested LLPS is obtained due to the interplay of the LLPS binodal with glass formation. Based on the results on the kinetics presented above, we can reach the following main conclusions.

Firstly, the growth kinetics of the characteristic length  $\xi$  strongly depends on the quench depth: for shallow quenches it follows the classical diffusive coarsening  $\xi \sim t^{1/3}$ , while for deep quenches the value of  $\xi$  is almost stationary and the phase separation can be considered arrested. The kinetics can be slowed down by lowering the temperature or increasing the overall protein and PEG concentration. For intermediate quench depths, we observe a three-stage growth kinetics, *i.e.* an initial coarsening followed by a slowdown plateau, then by a resumption of the coarsening. The system following this type of growth kinetics can undergo a temporarily arrested state.

Secondly, we note that this growth behavior also exists in a BSA-YCl<sub>3</sub> system exhibiting a LCST phase behavior, suggesting a rather universal growth kinetics in systems approaching the arrested state. The temporary nature of the arrested state is most likely due to the asymmetric (off-critical) quench. In this case the minority phase is the dilute phase, which can still

coarsen through the glassy majority phase. This is consistent with earlier simulation results, while a role of aging and collapse cannot be completely ruled out.

Finally, despite the potential mechanisms discussed in this work, our understanding of the temporarily arrested state at the molecular level is far from clear. Migration-coalescence through a glassy phase, intermittent coarsening, aging and collapse may all contribute to different extents to the global kinetics observed. We hope that our experimental study will inspire further efforts for a full theoretical understanding.

## Conflicts of interest

There are no conflicts to declare.

## Acknowledgements

We would like to thank Dr Vitaliy Pipich (JCNS) for his help with the VSANS setup, Prof. Brian B. Laird (University of Kansas) for the useful literature suggestions, Prof. Thilo Stehle (IFIB, University of Tübingen) for sharing lab resources. Additionally, we acknowledge Mayank Chugh, Patrizia Ricca and Salome Wörner for helpful assistance. The authors gratefully acknowledge the financial support provided by JCNS to perform the neutron scattering measurements at the Heinz Maier-Leibnitz Zentrum (MLZ), Garching, Germany, and the ESRF and Forschungszentrum Jülich/MLZ for the allocation of beamtimes. This work was supported by the DFG.

## References

- 1 A. Lomakin, N. Asherie and G. B. Benedek, *Proc. Natl. Acad. Sci. U. S. A.*, 1999, **96**, 9465–9468.
- 2 H. Liu, S. K. Kumar and F. Sciortino, *J. Chem. Phys.*, 2007, **127**, 084902.
- 3 F. Roosen-Runge, F. Zhang, F. Schreiber and R. Roth, *Sci. Rep.*, 2014, **4**, 7016.
- 4 Y. Wang, A. Lomakin, R. F. Latypov, J. P. Laubach, T. Hideshima, P. G. Richardson, N. Munshi, K. Anderson and G. B. Benedek, *J. Chem. Phys.*, 2013, **139**, 121904.
- 5 A. S. Raut and D. S. Kalonia, *Mol. Pharmaceutics*, 2016, **13**, 1431–1444.
- 6 A. Sauter, F. Roosen-Runge, F. Zhang, G. Lotze, A. Feoktystov, R. M. J. Jacobs and F. Schreiber, *Faraday Discuss.*, 2015, **179**, 41–58.
- 7 U. Shimanovich, G. Bernardes, T. Knowles and A. Cavaco-Paulo, *Chem. Soc. Rev.*, 2014, **43**, 1361–1371.
- 8 T. Gibaud, N. Mahmoudi, J. Oberdisse, P. Lindner, J. S. Pedersen, C. L. P. Oliveira, A. Stradner and P. Schurtenberger, *Faraday Discuss.*, 2012, **158**, 267.
- 9 N. Mahmoudi and A. Stradner, *J. Phys. Chem. B*, 2015, **119**, 15522–15529.
- 10 S. Grouazel, J. Perez, J.-P. Astier, F. Bonneté and S. Veessler, *Acta Crystallogr., Sect. D: Biol. Crystallogr.*, 2002, **58**, 1560–1563.

- 11 Q. Chen, P. G. Vekilov, R. L. Nagel and R. E. Hirsch, *Biophys. J.*, 2004, **86**, 1702–1712.
- 12 D. Vivarès and F. Bonneté, *J. Phys. Chem. B*, 2004, **108**, 6498–6507.
- 13 Y. Wang and O. Annunziata, *J. Phys. Chem. B*, 2007, **111**, 1222–1230.
- 14 J. Möller, S. Grobelny, J. Schulze, S. Bieder, A. Steffen, M. Erlkamp, P. Michael, M. Tolan and R. Winter, *Phys. Rev. Lett.*, 2014, **112**, 028101.
- 15 F. Cardinaux, T. Gibaud, A. Stradner and P. Schurtenberger, *Phys. Rev. Lett.*, 2007, **99**, 118301.
- 16 A. Zaccone, J. J. Crassous and M. Ballauff, *J. Chem. Phys.*, 2013, **138**, 104908.
- 17 A. I. Campbell, V. J. Anderson, J. S. van Duijneveldt and P. Bartlett, *Phys. Rev. Lett.*, 2005, **94**, 208301.
- 18 K. Kroy, M. E. Cates and W. C. K. Poon, *Phys. Rev. Lett.*, 2004, **92**, 148302.
- 19 P. J. Lu, E. Zaccarelli, F. Ciulla, A. B. Schofield, F. Sciortino and D. A. Weitz, *Nature*, 2008, **453**, 499–503.
- 20 M. Miller and D. Frenkel, *Phys. Rev. Lett.*, 2003, **90**, 135702.
- 21 P. N. Segrè, V. Prasad, A. B. Schofield and D. A. Weitz, *Phys. Rev. Lett.*, 2001, **86**, 6042–6045.
- 22 A. P. Eberle, N. J. Wagner and R. Castañeda-Priego, *Phys. Rev. Lett.*, 2011, **106**, 105704.
- 23 N. E. Valadez-Pérez, Y. Liu, A. P. R. Eberle, N. J. Wagner and R. Castañeda-Priego, *Phys. Rev. E: Stat., Nonlinear, Soft Matter Phys.*, 2013, **88**, 060302.
- 24 G. Foffi, C. D. Michele, F. Sciortino and P. Tartaglia, *Phys. Rev. Lett.*, 2005, **94**, 078301.
- 25 J. W. Cahn, *J. Chem. Phys.*, 1965, **42**, 93–99.
- 26 J. K. Dhont, *J. Chem. Phys.*, 1996, **105**, 5112–5125.
- 27 S. Bhat, R. Tuinier and P. Schurtenberger, *J. Phys.: Condens. Matter*, 2006, **18**, L339.
- 28 E. D. Siggia, *Phys. Rev. A: At., Mol., Opt. Phys.*, 1979, **20**, 595–605.
- 29 L. F. Cugliandolo, *C. R. Phys.*, 2015, **16**, 257–266.
- 30 A. A. Nepomnyashchy, *C. R. Phys.*, 2015, **16**, 267–279.
- 31 W. Shi, W. Liu, J. Yang, Z. He and C. C. Han, *Soft Matter*, 2014, **10**, 2649–2655.
- 32 J. M. Subir, K. Das and S. Roy, *C. R. Phys.*, 2015, **16**, 303–315.
- 33 D. Aarts, R. Dullens and H. Lekkerkerker, *New J. Phys.*, 2005, **7**, 40.
- 34 L. J. Teece, M. A. Faers and P. Bartlett, *Soft Matter*, 2011, **7**, 1341–1351.
- 35 C. P. Royall, J. Eggers, A. Furukawa and H. Tanaka, *Phys. Rev. Lett.*, 2015, **114**, 258302.
- 36 R. Harich, T. Blythe, M. Hermes, E. Zaccarelli, A. Sederman, L. F. Gladden and W. C. K. Poon, *Soft Matter*, 2016, **12**, 4300–4308.
- 37 J. Sabin, A. E. Bailey and B. J. Frisken, *Soft Matter*, 2016, **12**, 5325–5333.
- 38 D. Sappelt and J. Jäcke, *Europhys. Lett.*, 1997, **37**, 13.
- 39 D. Sappelt and J. Jäcke, *Phys. A*, 1997, **240**, 453–479.
- 40 I. Zhang, C. P. Royall, M. A. Faers and P. Bartlett, *Soft Matter*, 2013, **9**, 2076–2084.
- 41 V. Testard, L. Berthier and W. Kob, *J. Chem. Phys.*, 2014, **140**, 164502.
- 42 T. Gibaud and P. Schurtenberger, *J. Phys.: Condens. Matter*, 2009, **21**, 322201.
- 43 S. Bucciarelli, L. Casal-Dujat, C. De Michele, F. Sciortino, J. Dhont, J. Bergenholtz, B. Farago, P. Schurtenberger and A. Stradner, *J. Phys. Lett.*, 2015, **6**, 4470–4474.
- 44 S. Da Vela, M. K. Braun, A. Dörr, A. Greco, J. Möller, Z. Fu, F. Zhang and F. Schreiber, *Soft Matter*, 2016, **12**, 9334–9341.
- 45 J. M. Olais-Govea, L. López-Flores and M. Medina-Noyola, *J. Chem. Phys.*, 2015, **143**, 174505.
- 46 H. Guo, S. Ramakrishnan, J. L. Harden and R. L. Leheny, *J. Chem. Phys.*, 2011, **135**, 154903.
- 47 G. Brambilla, D. El Masri, M. Pierno, L. Berthier, L. Cipelletti, G. Petekidis and A. B. Schofield, *Phys. Rev. Lett.*, 2009, **102**, 085703.
- 48 G. Sun, Y. Wang, A. Lomakin, G. B. Benedek, H. E. Stanley, L. Xu and S. V. Buldyrev, *J. Chem. Phys.*, 2016, **145**, 194901.
- 49 Y. Wang, R. F. Latypov, A. Lomakin, J. A. Meyer, B. A. Kerwin, S. Vunnum and G. B. Benedek, *Mol. Pharmaceutics*, 2014, **11**, 1391–1402.
- 50 C. Kalonia, V. Toprani, R. Toth, N. Wahome, I. Gabel, C. R. Middaugh and D. B. Volkin, *J. Phys. Chem. B*, 2016, **120**, 7062–7075.
- 51 P. Kheddo, J. E. Bramham, R. J. Dearman, S. Uddin, C. F. van der Walle and A. P. Golovanov, *Mol. Pharmaceutics*, 2017, **14**, 2852–2860.
- 52 S. Da Vela, F. Roosen-Runge, M. W. A. Skoda, R. M. J. Jacobs, T. Seydel, H. Frielinghaus, M. Sztucki, R. Schweins, F. Zhang and F. Schreiber, *J. Phys. Chem. B*, 2017, **121**, 5759–5769.
- 53 V. J. Anderson and H. N. W. Lekkerkerker, *Nature*, 2002, **416**, 811–815.
- 54 F. C. Hay and O. M. Westwood, *Practical Immunology*, John Wiley & Sons, Fourth edn, 2002.
- 55 J. Pande, A. Lomakin, B. Fine, O. Ogun, I. Sokolinski and G. Benedek, *Proc. Natl. Acad. Sci. U. S. A.*, 1995, **92**, 1067–1071.
- 56 M. Grimaldo, F. Roosen-Runge, F. Zhang, T. Seydel and F. Schreiber, *J. Phys. Chem. B*, 2014, **118**, 7203–7209.
- 57 P. Van Vaerenbergh, J. Léonardon, M. Sztucki, P. Boesecke, J. Gorini, L. Claustre, F. Sever, J. Morse and T. Narayanan, *Proceedings of the 12th International Conference on Synchrotron Radiation Instrumentation-SRI2015*, 2016, p. 030034.
- 58 J. C. Labiche, O. Mathon, S. Pascarelli, M. A. Newton, G. G. Ferre, C. Curfs, G. Vaughan, A. Homs and D. F. Carreiras, *Rev. Sci. Instrum.*, 2007, **78**, 091301.
- 59 V. Pipich and Z. Fu, *Journal of Large-scale Research Facilities JLSRF*, 2015, **1**, 31.
- 60 V. Pipich, *QtikWS: user-friendly program for reduction, visualization, analysis and fit of SA(N)S data*, 2012, <http://www.qtikws.de>.
- 61 A. M. Kulkarni, A. P. Chatterjee, K. S. Schweizer and C. F. Zukoski, *J. Chem. Phys.*, 2000, **113**, 9863–9873.
- 62 E. J. Yearley, P. D. Godfrin, T. Perevozchikova, H. Zhang, P. Falus, L. Porcar, M. Nagao, J. E. Curtis, P. Gawande and R. Taing, *et al.*, *Biophys. J.*, 2014, **106**, 1763–1770.
- 63 H. N. W. Lekkerkerker and R. Tuinier, *Colloids and the Depletion Interaction*, Springer, Netherlands, 2011.
- 64 T. Pérez, Y. Liu, W. Li, J. Gunton and A. Chakrabarti, *Langmuir*, 2011, **27**, 11401–11408.

- 65 Y. Wang, A. Lomakin, R. F. Latypov and G. B. Benedek, *Proc. Natl. Acad. Sci. U. S. A.*, 2011, **108**, 16606–16611.
- 66 H. Furukawa, *Adv. Phys.*, 1985, **34**, 703–750.
- 67 H. Tanaka, *J. Phys.: Condens. Matter*, 2000, **12**, R207.
- 68 P. Lindner and T. Zemb, *Neutrons, X-rays, and Light: Scattering Methods Applied to Soft Condensed Matter*, Elsevier, North-Holland, 2002.
- 69 P. Chaudhuri and J. Horbach, *J. Stat. Mech.: Theory Exp.*, 2016, **2016**, 084005.
- 70 E. Johnson, S. Prokofjev, V. Zhilin and U. Dahmen, *Zeitschrift für Metallkunde*, 2005, **96**, 1171–1180.
- 71 E. Johnson, S. Steenstrup, M. Levinsen, V. Prokofjev, V. Zhilin and U. Dahmen, *J. Mater. Sci.*, 2005, **40**, 3115–3119.